

Vibrational spectroscopy of the hydrated hydronium cluster ions $\text{H}_3\text{O}^+ \cdot (\text{H}_2\text{O})_n$ ($n = 1, 2, 3$)

L. I. Yeh, M. Okumura,^{a)} J. D. Myers,^{b)} J. M. Price, and Y. T. Lee

Department of Chemistry, University of California, Berkeley, California 94720 and Materials and Chemical Sciences Division, Lawrence Berkeley Laboratory, Berkeley, California 94720

(Received 24 January 1989; accepted 6 July 1989)

The gas phase infrared spectra of the hydrated hydronium cluster ions $\text{H}_3\text{O}^+ \cdot (\text{H}_2\text{O})_n$ ($n = 1, 2, 3$) have been observed from 3550 to 3800 cm^{-1} . The new spectroscopic method developed for this study is a two color laser scheme consisting of a tunable cw infrared laser with 0.5 cm^{-1} resolution used to excite the O–H stretching vibrations and a cw CO_2 laser that dissociates the vibrationally excited cluster ion through a multiphoton process. The apparatus is a tandem mass spectrometer with a radio frequency ion trap that utilizes the following scheme: the cluster ion to be studied is first mass selected; spectroscopic interrogation then occurs in the radio frequency ion trap; finally, a fragment ion is selected and detected using ion counting techniques. The vibrational spectra obtained in this manner are compared with that taken previously using a weakly bound H_2 “messenger.” A spectrum of H_7O_3^+ taken using a neon messenger is also presented. *Ab initio* structure and frequency predictions by Remington and Schaefer are compared with the experimental results.

INTRODUCTION

Properties of the hydrated hydronium ions are of broad interest in chemistry.¹ The hydronium ion and its hydrated analogs are present throughout our natural environment. Narcisi and Bailey identified H_3O^+ and H_5O_2^+ in the *D* region of the ionosphere in their pioneering rocket-borne mass-spectrometer flights.² Since then, it has been shown that $\text{H}_3\text{O}^+ \cdot (\text{H}_2\text{O})_n$ ions are the dominant ions in the *D* region.³ Not only are water cluster ions important in atmospheric studies, they are also important components of aqueous solutions and govern the proton transfer process.

Much of the early work attempted to determine the structure of these ions in crystals by using x-ray^{4–6} or neutron diffraction^{6–8} data. Soon after Nakahara, Saito, and Kuroya first suggested the existence of H_5O_2^+ in crystals of organic acids,⁹ a central question became whether this ion existed as the asymmetric $\text{H}_3\text{O}^+ \cdot \text{H}_2\text{O}$ structure or the symmetric $\text{H}_2\text{O} \cdot \text{H}^+ \cdot \text{OH}_2$ structure. Evidence to support both conclusions was found among the many crystal environments studied.^{7,8}

Spectroscopic work was also initially constrained to liquid or crystalline phases. Infrared absorption was used to confirm the presence of dioxonium ion (H_5O_2^+) in several different salts.¹⁰ One of the earliest IR spectra of H_9O_4^+ was taken in the HBr crystalline hydrate.¹¹ Many other spectroscopic studies soon followed.^{12–17} All of these studies shared the problems of low resolution and ambiguity in assigning absorption features.

Gas phase studies were carried out on the formation of hydrated protons by Searcy and Fenn, who used a quadrupole mass spectrometer to detect $\text{H}^+ (\text{H}_2\text{O})_n$ ($n = 1–28$) formed in a corona discharge source.¹⁸ Lancaster *et al.* de-

tected large water clusters of $n = 1–180$ from the secondary ion mass spectrum of ice.¹⁹ Beuhler and Friedman used mass spectrometric detection to study formation of water cluster ions with $m/e < 59\,000$.²⁰ Important thermodynamic work was done by Kebarle's group in studying the temperature dependence of the equilibrium constants for reactions involving the successive addition of a water molecule to determine heats of reaction. They obtained binding energies of $\text{H}_3\text{O}^+ \cdot (\text{H}_2\text{O})_n$ to be 31.6, 19.5, and 17.9 kcal/mol (11 050, 6820, and 6260 cm^{-1}) for $n = 1, 2,$ and 3 , respectively.^{21–23} An independent investigation by Meot-Ner and Field found binding energies of 33.0, 21.0, and 16.0 kcal/mol for $n = 1, 2,$ and 3 , respectively.²⁴

The first gas phase spectroscopic work on the hydrated hydronium ions was carried out by Schwarz using the pulsed radiolysis method.²⁵ Absorption spectra from 2000–4000 cm^{-1} of the ions $\text{H}_3\text{O}^+ \cdot (\text{H}_2\text{O})_n$ ($n = 3, 4, 5$) were obtained at 40 cm^{-1} resolution. Although various ions are expected to be formed in a pulsed radiolysis experiment, the relative abundances of different size clusters can be changed by varying the partial pressure of water vapor. Equilibrium constants from Kebarle *et al.*²¹ were used to estimate these abundances and decompose the data into individual spectra for each cluster ion. Spectral features assigned to H_9O_4^+ occurred at 3710 and 3620 cm^{-1} , corresponding to the antisymmetric and symmetric modes of the three outer water molecules, and at 3000 and 2660 cm^{-1} , corresponding to the symmetric and antisymmetric modes of the central H_3O^+ .

High-resolution infrared absorption spectra have recently been obtained on the predecessor of these ions H_3O^+ .^{26–31} The inversion splitting of the ground state was found to be 55.3 cm^{-1} .^{29–31} These experimental searches were complemented by extensive theoretical efforts.^{32–35}

Many theoretical efforts have also attempted to determine the structure and vibrational spectra of the layer hydrated hydronium ions.^{36–38} For example, self-consistent field (SCF)-LCGO calculations by Potier, Leclercq, and

^{a)} Current address: Chemistry Department, California Institute of Technology, Pasadena, CA 91125.

^{b)} NSF predoctoral fellowship.

Allavena found H_5O_2^+ to have C_2 symmetry.³⁹ They systematically varied the $\angle\text{HOH}$ of the two end waters, the angle between the O–O direction and the bisecting line of the $\angle\text{HOH}$ angle, and the relative orientation of the two water groups to find the lowest energy structure. They calculated a barrier height of ~ 1.1 kcal/mol for rotation of the end waters and ~ 1.2 kcal/mol to bend the plane of the end water groups. The binding energy of H_5O_2^+ relative to the sum of the energies for separated H_2O and H_3O^+ was found to be 32.06 kcal/mol. Potier *et al.* also addressed the ease with which the H_5O_2^+ structure adjusts to its environment. They report that the range of experimental structures found in crystals are practically all within kT of the lowest energy structure. Unpublished results by Remington and Schaefer predict structures and vibrational frequencies and intensities for $\text{H}_3\text{O}^+ \cdot (\text{H}_2\text{O})_n$ ($n = 1, 2, 3$).⁴⁰ Their calculations were done at the SCF level using a double zeta plus polarization (DZP) basis set for all three ions. In addition, H_5O_2^+ was treated at the configuration interaction level including single and double (CISD) excitations with a DZP basis set. Calculated

structures at the highest level of theory used for these three water cluster ions are shown in Fig. 1. The two lowest energy structures for each species are shown. These cluster ions can be viewed as an H_3O^+ core which has been solvated by H_2O groups. This interpretation of the structures becomes more accurate as the cluster size increases.

Studying the vibrational spectroscopy of cluster ions, such as the hydrated hydronium ions $\text{H}_3\text{O}^+ \cdot (\text{H}_2\text{O})_n$ is an inherently difficult problem. Although one may study these species in the liquid phase or in a gas cell where their densities are relatively high, these methods have the disadvantage of ambiguity in assigning absorption features to a given species (see, e.g., Ref. 25). The velocity modulation technique⁴¹ in gaseous discharge plasmas has provided important information on high-resolution infrared absorption spectra of molecular ions, but weakly bound ionic clusters are nearly impossible to study in high temperature plasmas, even if they can be formed with high densities. This is due to the large density of states that dilutes the population in any given state. Ion beams have the potential of being much colder

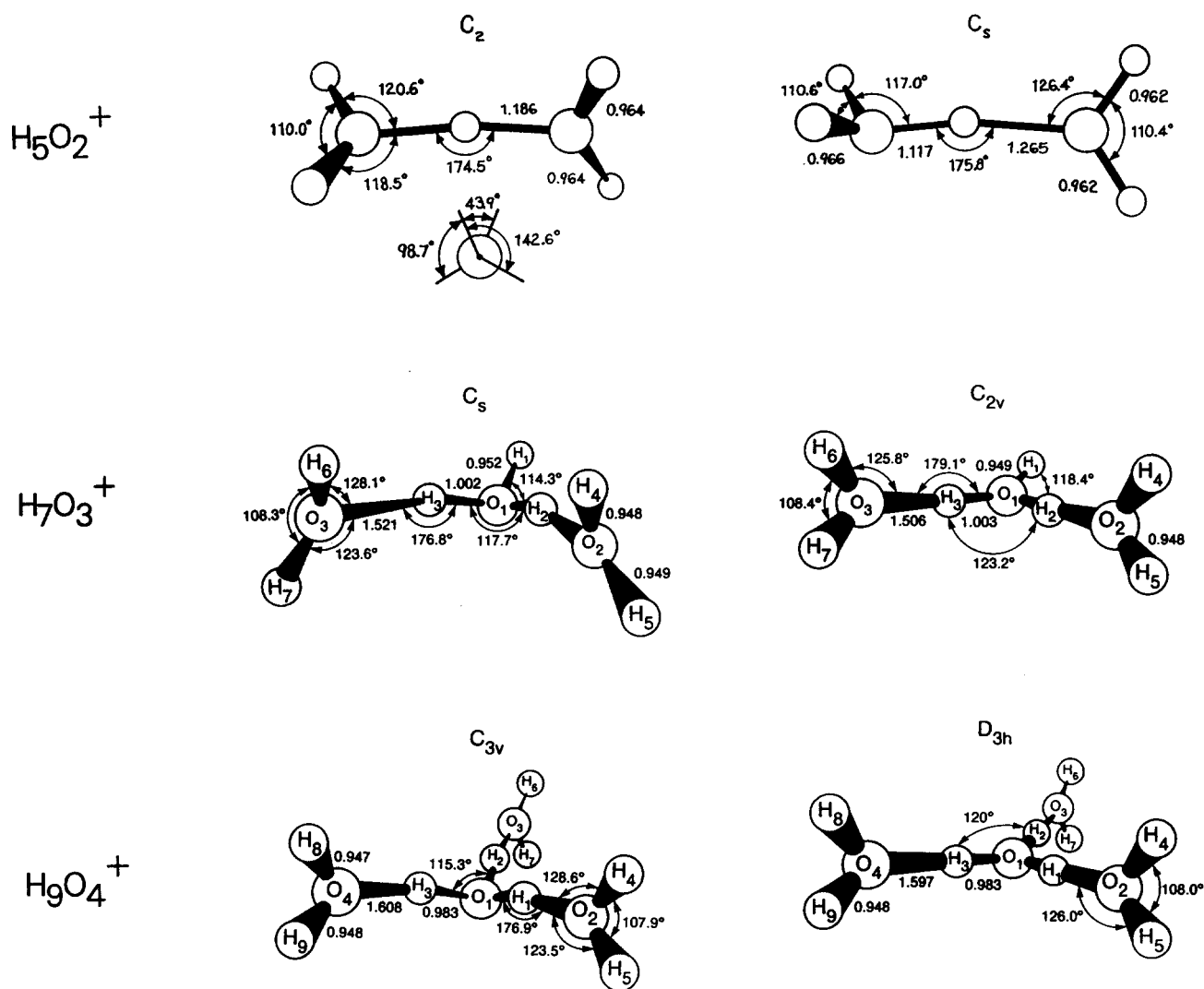


FIG. 1. Lowest energy structures calculated for H_5O_2^+ , H_7O_3^+ , and H_9O_4^+ by Remington and Schaefer. The column on the left shows the structures predicted to be the lowest in energy. See the text for details. From Ref. 40.

than discharges since a supersonic expansion can be used. In addition, they also have the advantage of mass selection capability, but at the expense of orders of magnitude in ion density. In most cases, this makes traditional absorption spectroscopy impossible.⁴² Thus, one has to depend on the observation of the consequence of photon absorption, rather than the attenuation of photon intensity due to absorption, when performing cluster ion spectroscopy.

For very weakly bound ionic clusters such as H_5^+ , H_7^+ , H_9^+ , etc., excitation of vibrational degrees of freedom induces dissociation and one can see the vibrational predissociation process to obtain vibrational spectra,^{43,44} as has been done in the investigation of neutral molecular clusters,^{45,46} but there are many cluster ions, such as the hydrated hydronium ions, whose binding energy far exceeds the energy of vibrational quanta, and the vibrational predissociation process will not occur after excitation of the fundamental molecular vibration. In our recent ion beam study of the hydrated hydronium ions, we have overcome this obstacle by utilizing two complementary techniques. Both methods take advantage of the inherently high sensitivity of ion detection.

The first approach, which has been reported previously,⁴⁷⁻⁴⁹ is to attach a weakly bound "messenger" M to the hydrated hydronium ions. The attached messenger is hoped to have only a small effect on the spectrum. The scheme is as follows: A tunable infrared laser is used to excite the O-H stretch of the cluster ion. Intramolecular vibrational relaxation causes the cluster ion to undergo vibrational predissociation, losing the messenger. The role of the messenger is to indicate when an absorption has taken place. By monitoring the dissociation product as a function of laser frequency, the absorption spectra of these $H_3O^+ \cdot (H_2O)_n \cdot M$ ($n = 1, 2, 3$) ions have been found. Initially, hydrogen molecule was used as the messenger.⁴⁷⁻⁴⁹ More recently, spectra have been taken for $H_7O_3^+$ using neon as a messenger.⁵⁰

The second approach is to detect the vibrationally excited $H_3O^+ \cdot (H_2O)_n$ ($n = 1, 2, 3$) ions using an infrared multiphoton dissociation process. The procedure is to first excite from $v = 0$ to $v = 1$ in the O-H stretch using a tunable IR laser. We then make use of the fact that the density of states near $v = 0$ and $v = 1$ are very different for ionic clusters which contain many low frequency vibrations. The vibrationally excited cluster ions are likely to be in a region with a high enough density of states for sequential excitation by a fixed frequency laser. This means that one can distinguish between ground state and vibrationally excited $H_3O^+ \cdot (H_2O)_n$ by using a multiphoton dissociation (MPD) process to selectively dissociate the latter by eliminating one of the outer water molecules from the excited $H_3O^+ \cdot (H_2O)_n$ using a CO_2 laser. Once again, we monitor the dissociation product, in this case $H_3O^+ \cdot (H_2O)_{n-1}$, as a function of the excitation frequency of the first laser to get the absorption spectra of the $H_3O^+ \cdot (H_2O)_n$ ions. An extension of this approach is to use a single tunable pulsed laser to both excite and dissociate the cluster ions. This was feasible for $H_7O_3^+$ and $H_9O_4^+$, but not $H_5O_2^+$ as discussed below.

This paper presents the spectra of $H_5O_2^+$, $H_7O_3^+$, and $H_9O_4^+$ from 3550 to 3800 cm^{-1} and compares them to the

spectra of $H_5O_2^+ \cdot H_2$, $H_7O_3^+ \cdot H_2$, $H_9O_4^+ \cdot H_2$,⁴⁷⁻⁴⁹ and $H_7O_3^+ \cdot Ne$.⁵⁰ A comparison with vibrational frequencies calculated using *ab initio* methods by Remington and Schaefer⁴⁰ is also made and implications regarding the structures and the messenger binding sites are discussed.

EXPERIMENTAL DETAILS

The ionic clusters are produced in a high pressure corona discharge source^{18,20,51} as shown in Fig. 2. Typical discharge conditions behind the nozzle are 1.2 kV from cathode to anode, 20–40 μA discharge current, and 200 Torr of H_2 gas containing trace amounts of H_2O . For these experiments, the body of the source itself was not cooled and was probably only slightly above room temperature due to heat from the discharge. The cathode, which is floated at 350 V, is the copper wall of the source which is located 0.150 ± 0.003 in. away from the nickel plated iron needle which serves as the anode. The nozzle, which is silver soldered into the source body, is therefore also floated at 350 V. The beam containing various ionic clusters is formed by expanding the plasma through a 75 μm nozzle.

The proton affinity of H_2O is 167 kcal/mol, which is 66 kcal/mol higher than that of the carrier gas H_2 .⁵² Therefore, protonated water ions will be the dominant ion species even with very little neutral water present. Because only trace amounts of water are necessary for this experiment, we found the residual water on the walls of the 1/4 in. copper tubing was sufficient as the source of water. In fact, even this was too much, even though the inlet line was routinely pumped and Matheson ultrahigh purity H_2 (99.999%) was generally used. Therefore, a molecular sieve trap filled with Linde 13X 1/8 in. pellets was used in the inlet line. For $H_5O_2^+$, the sieve trap was cooled using liquid nitrogen. $H_7O_3^+$ production was optimized with the sieve trap cooled in an ice bath. The larger $H_9O_4^+$ cluster was produced in

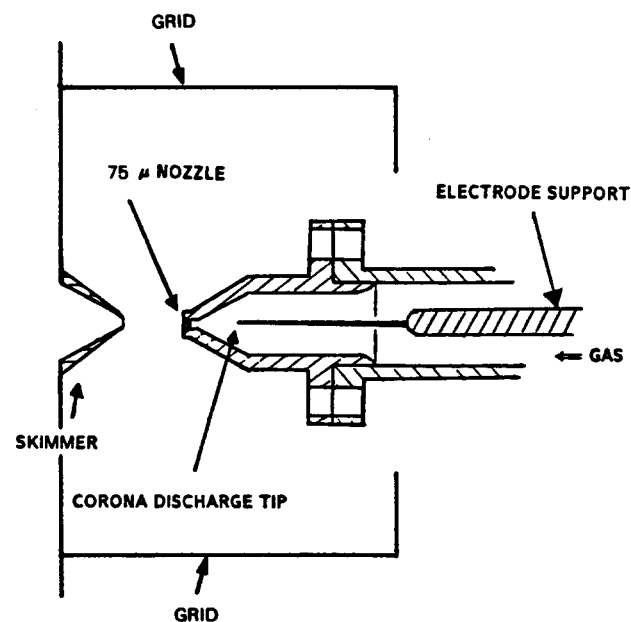


FIG. 2. A schematic of the corona discharge ion source.

large quantities by bypassing the sieve trap and running the gas directly into the source.

Downstream from the nozzle by 6.4 mm is a 1.5 mm diameter skimmer which is floated such that the difference in potential between the nozzle and skimmer is 1 V or less. This weak field will allow the ions to drift toward the skimmer, but also prevent excessive collisional heating of the nascent cluster ions. A grid which is also floated at 350 V surrounds the nozzle/skimmer area to keep this area relatively fieldfree. The pressure in the chamber before the skimmer is $1\text{--}2 \times 10^{-4}$ Torr under operating conditions.

After the skimmer, the ions pass into a second differential region, with pressures normally at least an order of magnitude lower than in the first region. Here, they are focused and deflected in one of two possible directions. One direction is toward a quadrupole mass filter with an electron multiplier system which is used for easier source characterization and optimization. The other direction, which leads to the section where spectroscopic investigation is carried out, is to a third differential region (at 2×10^{-8} Torr), where mass selection is achieved using a 60° sector magnet. The mass resolution of the sector magnet is about $M/\Delta M \approx 150$. To aid in achieving high transmission, a set of quadrupole lens pairs is placed before and after the magnet.⁵³⁻⁵⁶ A 3.2 mm inner diameter tube, 36 mm long, leads to the ultrahigh vacuum section of the machine, which has a pressure generally about 1×10^{-9} Torr. A schematic of the apparatus is shown in Fig. 3.

Upon entering the UHV region, the ion of interest is bent 90° by an electrostatic quadrupole field deflector.⁵⁷ There are two major advantages to this selection. First, by choosing an electrostatic deflector, all masses with the same energy will be transmitted along the same trajectory. Second, the quadrupole field deflector geometry has its rods spaced such that the laser beam can exit the machine without hitting the electrodes.

The ions are then decelerated from 350 to about 5 V and focused into a 50-cm-long radiofrequency octopole ion trap. The energy of the ions in the trap is ≤ 0.5 eV. The ion trap consists of eight molybdenum rods of 0.32 cm diameter

evenly spaced on a 1.25 cm diameter circle. An rf voltage of 7.4 MHz and 200–300 V peak to peak is applied with adjacent rods having opposite phases. While the ions are trapped, they interact with a tunable infrared laser. Additional experimental details can be found in Ref. 58.

Two different laser schemes were needed depending on the approach taken. When studying $\text{H}_3\text{O}^+ \cdot (\text{H}_2\text{O})_n \cdot M$, a single tunable infrared laser was needed.⁴⁷⁻⁵⁰ The system used was a Quanta-Ray infrared wavelength extender (IR-WEX). The IR-WEX generates infrared at the difference between the fundamental of a YAG laser and the output from a pulsed dye laser. The laser path between the output of the tunable infrared laser and the entrance of the machine was enclosed and continually flushed with dry nitrogen to reduce atmospheric water absorptions in both laser schemes.

The second laser scheme consists of two lasers and is used to investigate the more strongly bound $\text{H}_3\text{O}^+ \cdot (\text{H}_2\text{O})_n$. The first laser is a Burleigh cw F-center laser (FCL) which is scanned from 3550 to 3800 cm^{-1} with a linewidth of 0.5 cm^{-1} . This is the region of an O–H stretching vibration. The second laser, used to dissociate the vibrationally excited H_5O_2^+ , H_7O_3^+ , or H_9O_4^+ ions through a multiphoton process, is an MPB Technologies Inc. cw CO_2 laser. A custom designed beam combiner on a ZnSe substrate (CVI Laser Corp.) is used to overlap spatially the FCL beam with the CO_2 beam. The frequency and intensity of the CO_2 laser is determined by trying to reach the ideal situation, where none of the ground state $\text{H}_3\text{O}^+ \cdot (\text{H}_2\text{O})_n$ ions absorb enough photons to dissociate, but those in $v = 1$ do dissociate late $\text{H}_3\text{O}^+ \cdot (\text{H}_2\text{O})_{n-1}$ and H_2O . This ideal situation is different for the three cluster ions studied and is described below.

In H_5O_2^+ , as opposed to H_7O_3^+ and H_9O_4^+ , the vibrationally excited ions do not readily absorb enough photons from the CO_2 laser to dissociate. In order to estimate the density of vibrational states, the direct count method with seven to nine frequency groups was used.⁵⁹ Around 3750 cm^{-1} , H_5O_2^+ is estimated to have 38 states/ cm^{-1} , H_7O_3^+ has 65 000 states/ cm^{-1} , and H_9O_4^+ has 2×10^8 states/ cm^{-1} . Thus, the density of states for H_5O_2^+ is rather sparse, and it is not in the quasicontinuum region, making the multi-

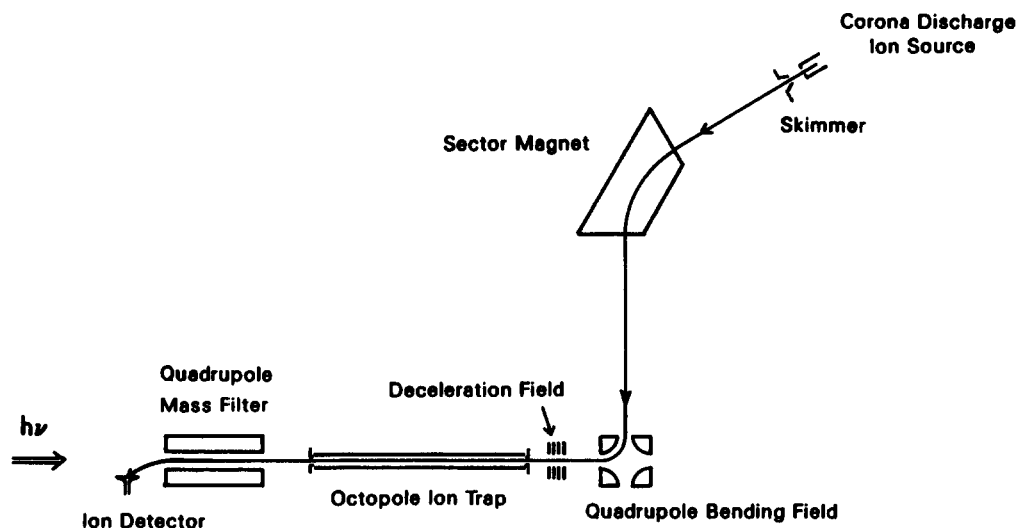


FIG. 3. A schematic of the experimental arrangement consisting of a radiofrequency ion trap and a tandem mass spectrometer.

photon dissociation process less facile. Therefore, the CO₂ laser is run full power (8 W out of the laser) on $R(24)$ of the $00^0_1-02^0_0$ transition. Since a cw CO₂ laser is used to irradiate continuously the octopole ion trap, the length of time the H₅O₂⁺ ions reside in the octopole ion trap is a third variable which is optimized to achieve a low H₃O⁺ background from those H₅O₂⁺ ions that do not absorb an IR photon from the F-center laser and a high H₃O⁺ signal from those H₅O₂⁺ that do. In this case, 100 ms was found to be optimal. The residence time of the ions and the laser intensity together determine the energy fluence of the laser irradiation of the ions in the trap. Both the F-center laser and the CO₂ laser were run cw into the ion trap of the machine. Typical ion counts of H₅O₂⁺ with a 100 ms trap time and at a sampling rate of 7.9 times per second were 2000–2500 cps. RRKM lifetimes of H₅O₂⁺ excited 0.1 kcal/mol above the dissociation limit are estimated to be < 1 μs.^{59,60}

When studying H₇O₃⁺, the CO₂ laser was set on $R(20)$ of the $00^0_1-10^0_0$ band. The laser power output was just over 6 W and power after the beam excited the machine through the electrostatic bending field electrodes was generally 2.2 W due to losses at each laser optic and during propagation of the laser beam through the machine. The trapping time chosen was 57.5 ms. A chopper was used to separate in time the FCL and CO₂ beams. The timing sequence, shown in Fig. 4, was as follows: The lens at the entrance of the octopole trap was gated low for 1.0 ms to allow the H₇O₃⁺ ions into the trap. The chopper then allowed the FCL into the trap for 25 ms. The CO₂ laser, starting 2.0 ms after the FCL was blocked, interacted with the ions for 30.5 ms. The lens at the exit of the octopole was then pulsed low for 5.0 ms to allow all of the ions out of the trap toward the detector. The trap is then readied for a new cycle. This gave 6000–9000 cps of mass-selected H₇O₃⁺ at the detector.

The CO₂ laser was run on the same line [$R(20)$ of $00^0_1-10^0_0$] for H₉O₄⁺. The intensity was attenuated by passing the beam through a gas cell containing ethylene. The gas cell was made out of brass with NaCl windows on either side placed at Brewster's angle in a nonparallel geometry to mini-

mize both reflection losses and beam walk. The CO₂ intensity after the gas cell was 2.0 W. Power measured at the opposite end of the machine was 0.6 W. Again, a trapping time of 57.5 ms was selected. The timing sequence used for H₉O₄⁺ was the same as that used with H₇O₃⁺. H₉O₄⁺ was the easiest ion to make and we obtained 30 000–40 000 cps at the detector after trapping.

The primary reason the chopper was not used in the H₅O₂⁺ experiment was the lower signal levels obtained when chopping. This is likely due to radiative relaxation of the initially excited O–H stretch before the CO₂ laser was unblocked. Radiative lifetimes for OH, OH⁻, and OH⁺ were calculated to be 82.0, 7.3, and 3.8 ms, respectively.⁶¹ Lifetimes in H₃O⁺ are calculated to be 0.5 ms for the ν_3 mode and 13–19 ms for the ν_1 mode.^{33,62} In H₂O, lifetimes calculated from infrared intensities are 240 and 13 ms for the symmetric and antisymmetric modes, respectively.⁶³ The radiative lifetimes of the stretches excited in H₅O₂⁺ should be between the values estimated for H₃O⁺ and H₂O if the energy of excitation does not transfer quickly to low-frequency modes. Of course, the minimal absorption of CO₂ photons by H₅O₂⁺ in the ground state allows us to use this continuous scheme. Otherwise, the spectra could be substantially contaminated by those H₅O₂⁺ which are first excited by a CO₂ photon.

A one color modification of this technique was successfully applied to H₇O₃⁺ and H₉O₄⁺. This scheme used the pulsed IR-WEX to provide both the photon to excite the O–H stretch and the subsequent photons needed to dissociate the cluster ions.

After the laser irradiation, all of the ions are ejected from the rf ion trap. It is the creation of fragment ions, not the decrease of parent ions, which is monitored by an Extra-nuclear quadrupole mass filter equipped with a Daly-type ion detector.⁶⁴ Specifically, when studying H₅O₂⁺ · H₂, the quadrupole mass filter selects H₅O₂⁺ fragment ions; when studying H₅O₂⁺, and H₃O⁺ ions are mass selected. By monitoring the fragment ion signal as a function of the tunable IR laser frequency, the vibrational spectrum is obtained.

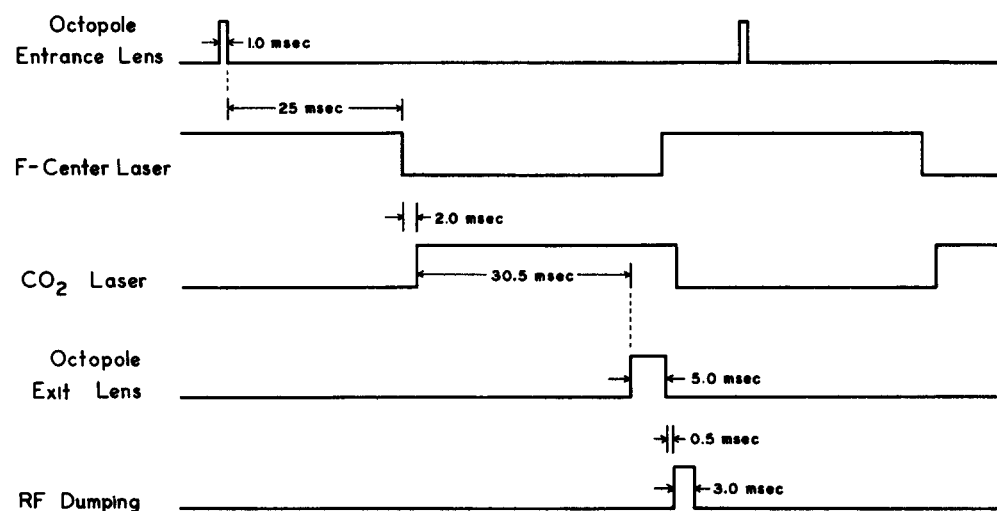


FIG. 4. The timing sequence used in obtaining the spectra of H₇O₃⁺ and H₉O₄⁺. After the octopole entrance lens is gated to allow ions into the trap for 1.0 ms, the F-center laser interacts with the ions for 25.0 ms. 2.0 ms after the FCL is blocked, the CO₂ laser is unblocked for 30.5 ms. The ions are then let out of the trap by gating the exit lens low for 5.0 ms. The trap is then emptied and readied for a new cycle by dumping the rf.

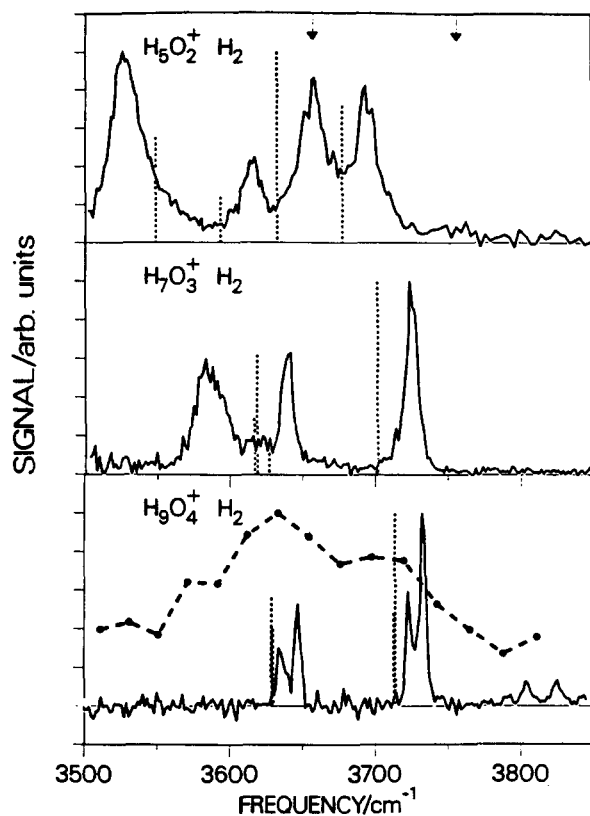


FIG. 5. Infrared spectra of $\text{H}_5\text{O}_2^+ \cdot \text{H}_2$, $\text{H}_7\text{O}_3^+ \cdot \text{H}_2$, and $\text{H}_9\text{O}_4^+ \cdot \text{H}_2$. In the top panel, the dashed lines correspond to the frequencies and intensities calculated in Ref. 40 for the C_s geometry of H_5O_2^+ . The arrows point to the locations of the symmetric and antisymmetric O–H stretches in H_2O . The dashed lines in the middle and lowest panels correspond to the frequencies for the lowest energy calculated structures for H_7O_3^+ and H_9O_4^+ , respectively. The dashed curve in the bottom panel shows the low-resolution spectrum for H_9O_4^+ obtained by Schwarz.

RESULTS AND ANALYSIS

The previously presented hydrated hydronium spectra obtained by using a hydrogen molecule as a messenger^{47–49} are shown in Fig. 5. Each spectrum will be compared in turn with the appropriate spectrum obtained without the perturbation by an H_2 .

H_5O_2^+

The smallest ion studied using the two color scheme was H_5O_2^+ . The infrared spectrum obtained from 3550 to 3770 cm^{-1} is presented in Fig. 6. Two features are seen. At lower frequency is a broad, featureless band centered at 3608.8 cm^{-1} with a width of $\sim 15 \text{ cm}^{-1}$. The higher frequency band, centered at 3684.4 cm^{-1} is composed of many peaks, separated by $\sim 11.6 \text{ cm}^{-1}$. Contrast this spectrum with the $\text{H}_5\text{O}_2^+ \cdot \text{H}_2$ spectrum shown in Fig. 5. Rather than two features, four are now evident with two of these bands being centered within 8 cm^{-1} of the two bands seen in the H_5O_2^+ spectrum. The very dissimilar spectra calls into question the validity of using H_2 as a messenger to obtain the spectrum of H_5O_2^+ .

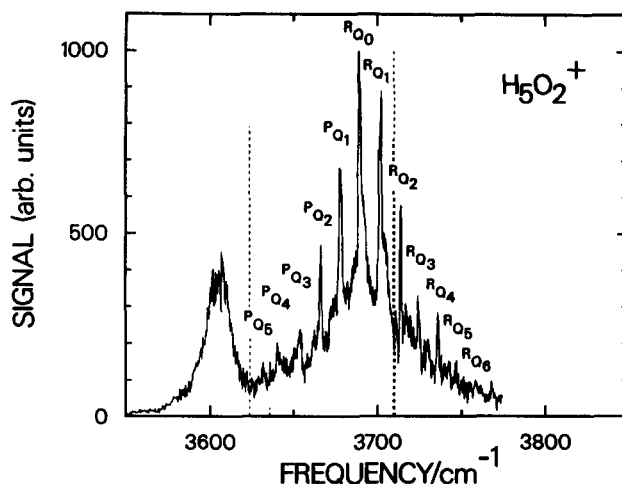


FIG. 6. The infrared spectrum of H_5O_2^+ obtained using the two color IRMPD technique. The dashed lines correspond to the frequencies and intensities calculated in Ref. 40 for the C_2 symmetry structure.

To understand the origin of the disparate spectra, one needs to consider the possible structures of H_5O_2^+ . Remington and Schaefer calculated structures, energies, and frequencies for H_5O_2^+ at both the SCF and CISD levels. Two structures, which are very close in energy at both levels, are the C_s and C_2 structures as seen in Fig. 1. One of the primary differences between them is that the C_2 structure has a H in the center, making it resemble two H_2O units equally sharing a proton, whereas the C_s structure has the central H off to one side, making the $\text{H}_3\text{O}^+ \cdot \text{H}_2\text{O}$ picture more appropriate. The other major difference is that, in the C_s structure the H_3O^+ is pyramidal, whereas in the C_2 structure, the $\text{H}_2\text{O} \cdot \text{H}^+$ is almost planar. The initial calculation, done at the SCF level with a DZP basis set, found the C_s geometry to be lower in energy by 0.27 kcal/mol. The higher level CISD, also with a DZP basis set, found the C_2 structure lower in energy by 0.19 kcal/mol. The geometries also changed. The $\text{H}_2\text{O} \cdot \text{H}^+$ portion in the C_2 structure is more pyramidal at the CISD level than at the SCF level, and the central proton for the C_s structure is closer to the center at the CISD level than at the SCF level. In addition to structures, vibrational frequencies and intensities were calculated for both the C_s and the C_2 geometries in the harmonic approximation with a semiempirical scaling factor.

The fact that the C_2 and C_s structures are separated in energy by less than 0.2 kcal/mol indicates that the potential is very flat and that there is almost no barrier to motion of the central proton from its center position to the side. The estimated binding energy of the H_2 molecule to the H_5O_2^+ , as discussed in Ref. 48, is less than 4 kcal/mol. This bond seems to be strong enough to shift the relative energies of the C_2 and C_s structures to favor the asymmetric C_s structure when the hydrogen molecule is attached.

This hypothesis is substantiated by comparing the spectra of H_5O_2^+ and $\text{H}_5\text{O}_2^+ \cdot \text{H}_2$ with the scaled frequencies calculated for the C_2 and C_s geometries. The two highest frequencies for the C_2 geometry, which correspond to antisymmetric O–H stretches of the two H_2O groups either

TABLE I. Vibrational frequencies for the hydrated hydronium ions. Experimental frequencies were found using the IRMPD technique and the messenger technique. Units are cm^{-1} .

	Experimental			Theory ^a		Assignment
	IRMPD	H ₂	Neon	Lower ^b	Higher ^c	
H ₅ O ₂ ⁺		3528			3549	H ₃ O ⁺ sym stretch, with H ₂ attached
	3608.8	3617		3624	3594	H ₂ O sym stretch
		3662			3633	H ₃ O ⁺ asym stretch
H ₇ O ₃ ⁺		3693		3710	3678	H ₂ O asym stretch
	3637.4	3642	3640	3619	3617	H ₂ O sym stretch
	3667.0	3587	3658	3627	3662	H ₃ O ⁺ O–H stretch
H ₉ O ₄ ⁺		3726	3722	3702	3703	H ₂ O asym stretch
	3721.6	3726				
		3636				
H ₅ O ₂ ⁺		3648		3628	3630	H ₂ O sym stretch, out of phase
	3644.9	3648				
		3723				
	3730.4	3733		3714	3715	H ₂ O asym stretch, in phase

^a All of the calculations were by Remington and Schaefer and were done at the self-consistent field level except for the C₂ geometry for H₅O₂⁺. A DZP basis set was used. From Ref. 40.

^b This column gives the scaled frequencies for the lowest energy calculated structure, i.e., H₅O₂⁺: C₂, H₇O₃⁺: C_s, and H₉O₄⁺: C_{3v}.

^c This column gives the scaled frequencies for the structure calculated to be second lowest in energy, i.e., H₅O₂⁺: C_s, H₇O₃⁺: C_{2v}, and H₉O₄⁺: D_{3h}.

in phase or out of phase, are predicted to have the same frequency. The next two highest frequencies for the C₂ geometry correspond to the symmetric O–H stretch in and out of phase. While they are predicted to be separated by 12 cm^{-1} , the intensity for the out of phase mode is predicted to be > 30 times larger than the in-phase mode. Thus, theory predicts only three strong bands in this frequency region, two of which are degenerate. This is in agreement with the experimental H₅O₂⁺ spectrum. The symmetric O–H stretch, calculated to occur at 3624 cm^{-1} , is seen at 3609 cm^{-1} . The antisymmetric O–H stretch, which is calculated at 3710 cm^{-1} , was found at 3684 cm^{-1} . These values are listed in Table I. The red shift from the symmetric and antisymmetric O–H stretches, as seen in free water compared to the experimentally observed peaks, is 48 and 72 cm^{-1} , respectively.

The spectrum of H₅O₂⁺·H₂ cannot be fully assigned by comparing to either the H₅O₂⁺ spectrum or the calculated frequencies for the C₂ geometry. Rather, the frequencies calculated using a C_s geometry, where the H₅O₂⁺ can be considered as an H₃O⁺·H₂O, fit the messenger spectrum better. The frequencies at 3617 and 3693 cm^{-1} have been assigned to the symmetric and antisymmetric O–H stretch of the H₂O moiety and are ~20 cm^{-1} higher than predicted by theory. The band at 3662 cm^{-1} , which is about ~30 cm^{-1} higher than theoretically predicted, is assigned primarily to a free O–H stretch of the H₃O⁺ and is an asymmetric stretch. The fourth band at 3528 cm^{-1} , however, is lower than theory by ~20 cm^{-1} . This band has also been assigned to a free O–H of H₃O⁺, but is a symmetric stretch.

In order to understand the origin of the sharp peaks seen in the 3684.4 cm^{-1} feature of H₅O₂⁺, it is helpful to realize that H₅O₂⁺ is a near symmetric top. The rotational constants from the calculated C₂ structure are $A = 6.120$, $B = 0.2936$, and $C = 0.2923 \text{ cm}^{-1}$. The progression seen is characteristic of a perpendicular band progression, where the transition moment lies perpendicular to the symmetric top axis which

lies along the O–H–O bond. Theory predicts two transitions at the same frequency of symmetry species *A* and *B*, which would both give perpendicular bands, with an 8.6–6.5 intensity ratio. A perpendicular band would be dominated by a prominent series of *Q* branches from the different subbands, especially when $A \gg B$,⁶⁵ as in this case. The separation of the *Q* branches should be $2(A'-B')$ which is 11.65 cm^{-1} . This is in good agreement with the experimentally observed spacing of ~11.6 cm^{-1} . Thus, we have assigned the spectrum shown in Fig. 6 to a progression of *Q* branches using the notation as described by Herzberg.⁶⁵ (The superscript *P* or *R* indicates ΔK , the large *Q* gives ΔJ , and the subscript is the *K* value for the lower state.) The possibility exists that the assignments should be shifted one position, i.e., the peak currently assigned to the ^RQ₀ subband may actually be the ^PQ₁ subband. A rotational temperature in the *K* quantum number of ~40 K is found.

An estimate of the legitimacy of using the symmetric top approximation can be made by using the *b* asymmetry parameter.⁶⁶ Using rotational constants calculated by Remington and Schaefer,⁴⁰ we obtain $b = 1.1 \times 10^{-4}$. This will give, except for very high *J* states, correction terms well below the resolution we are capable of obtaining due to the Doppler width of the ions moving back and forth in the ion trap. The Doppler width can be obtained by estimating that most probable velocity in the trap. If an ion energy in the trap of 0.5 eV is used, which is actually an upper bound, a Doppler width of 0.028 cm^{-1} is obtained.⁶⁷

Doppler limited high-resolution spectra for the $K' = 1 \leftarrow K'' = 0$ and $K' = 2 \leftarrow K'' = 1$ subbands are now under investigation.

H₇O₃⁺

The infrared spectrum obtained when H₃O⁺ is solvated by two water groups is shown in Fig. 7. The three bands are

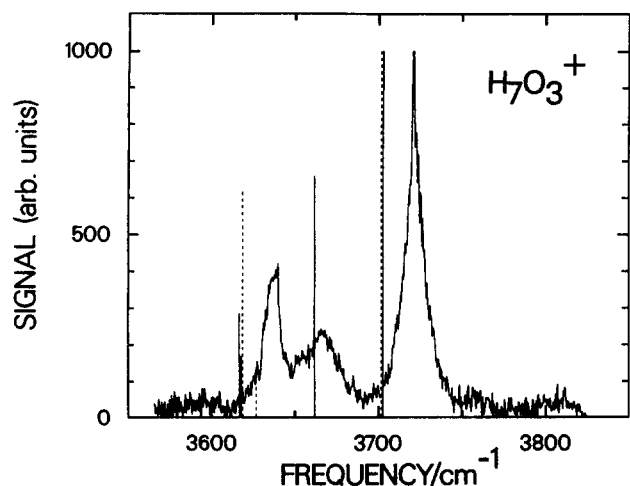


FIG. 7. The infrared spectrum of H_7O_3^+ obtained using the IRMPD method. Dashed lines correspond to the lowest energy C_s structure and solid lines to the C_{2v} structure.

located at 3637.4, 3667.0, and 3721.6 cm^{-1} . The bands at 3637.4 and 3721.6 cm^{-1} are assigned to the symmetric and antisymmetric O–H stretch of the outer water groups. The feature at 3667.0 cm^{-1} is due to the O–H stretch of the H_3O^+ core at the unoccupied site. The dashed lines in the figure correspond to the vibrational frequencies and intensities of the lowest energy C_s structure as calculated in Ref. 40. The solid lines correspond to the frequencies and intensities for the C_{2v} structure which is predicted to be higher in energy by 0.516 kcal/mol at the SCF level using a DZP basis set. The fact that the scaled frequencies from the C_{2v} geometry match our observed bands better implies that the C_{2v} structure may actually be the lowest energy geometry. Primary differences in the two structures are that in the C_s symmetry structure, the central H_3O^+ is more pyramidal and the O–H–O bond is slightly bent. The C_{2v} structure has a planar H_3O^+ core and a linear O–H–O bond. Both structures are shown in Fig. 1.

The spectrum for $\text{H}_7\text{O}_3^+ \cdot \text{H}_2$ is shown in Fig. 5. The three features are located at 3587, 3642, and 3726 cm^{-1} . The band at 3642 cm^{-1} , assigned to the symmetric O–H stretch of an outer water group, is only 5 cm^{-1} shifted from that seen in H_7O_3^+ . Similarly, the antisymmetric O–H stretch at 3726 cm^{-1} is shifted by less than 5 cm^{-1} from H_7O_3^+ . The third feature, however, has been shifted from 3667.0 to 3587 cm^{-1} , i.e. 80 cm^{-1} . This band corresponds to the O–H stretch of the unoccupied site of the H_3O^+ core. This shift leads us to conclude that the H_2 messenger is localized at this binding site.

Spectra taken of H_7O_3^+ by using neon as a messenger are presented in Fig. 8. The symmetric and antisymmetric O–H stretches are located at 3640.2 and 3722.3 cm^{-1} . The feature at 3640.2 cm^{-1} proves more interesting and was scanned more carefully as shown in Fig. 9. To the blue of the dominant feature at 3640.2 cm^{-1} are two shoulders. The first one, located at 3646.2 cm^{-1} , arises from leakage of H_9O_4^+ through the sector magnet. Neon was chosen as a messenger because we expected neon to perturb the spectrum much less

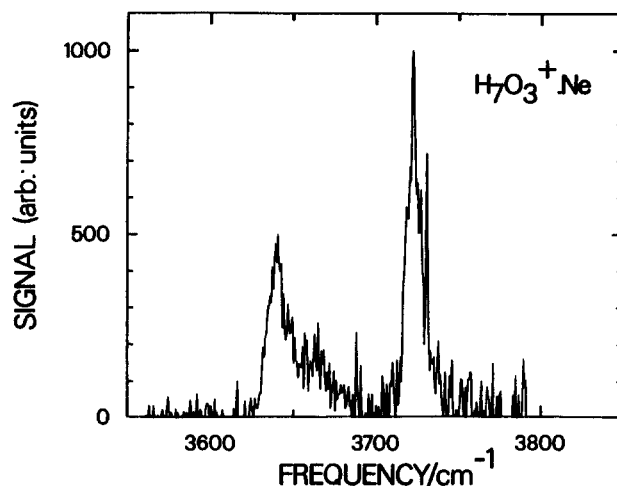


FIG. 8. The infrared spectrum of $\text{H}_7\text{O}_3^+ \cdot \text{Ne}$.

than H_2 , since it would be bound much more weakly. However, precisely because it is bound so weakly, it is very difficult to make $\text{H}_7\text{O}_3^+ \cdot \text{Ne}$. Therefore, even though $\text{H}_7\text{O}_3^+ \cdot \text{Ne}$ and H_9O_4^+ are separated by two mass units and even though the resolution of the sector magnet was approximately $M/\Delta M \approx 150$, the fact that generally we had at least two orders of magnitude more H_9O_4^+ than $\text{H}_7\text{O}_3^+ \cdot \text{Ne}$ explains why several percent of the purported $\text{H}_7\text{O}_3^+ \cdot \text{Ne}$ beam was actually H_9O_4^+ . The shoulder seen at 3646 cm^{-1} agrees within experimental uncertainty with the frequency of the symmetric O–H stretch of H_9O_4^+ at 3645 cm^{-1} as presented below. The corresponding H_9O_4^+ antisymmetric O–H stretch of an H_2O moiety is also present as the sharp feature at 3730 cm^{-1} .

The second shoulder, at 3657.8 cm^{-1} , is assigned to the O–H stretch of the H_3O^+ with the neon localized at the free binding site. As expected, neon does prove to be a much more subtle messenger than H_2 . The shift of the O–H stretch at this H_3O^+ site has been reduced from 80 to 9 cm^{-1} .

The spectra of H_7O_3^+ were taken by yet another meth-

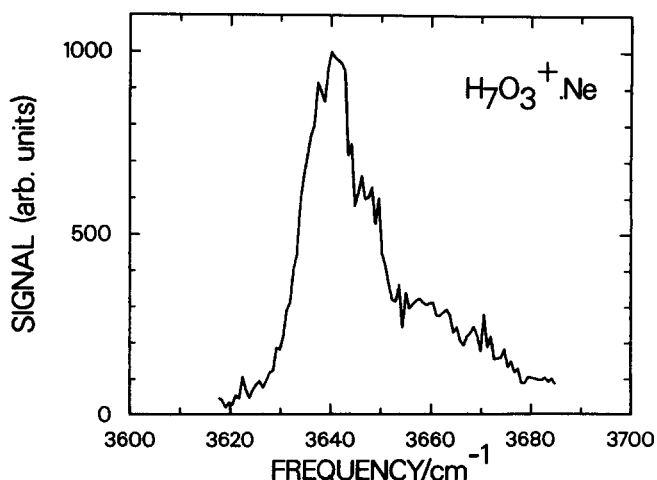


FIG. 9. Detail of the 3640 cm^{-1} feature in the spectrum of $\text{H}_7\text{O}_3^+ \cdot \text{Ne}$.

od. Rather than using the cw F -center laser followed by MPD using a cw CO_2 laser or using a messenger, a pulsed Infrared Wavelength Extender (IR-WEX) by Quanta Ray was used to obtain a MPD spectrum. The high peak powers generated by the pulsed IR laser made it possible for H_7O_3^+ to absorb more than one photon from this laser. The H_5O_2^+ fragment was again monitored as a function of the frequency of the IR-WEX laser. The spectrum consists of three bands located at 3637.4, 3664.6, and 3721.6 cm^{-1} , which are within experimental error of the positions found using the FCL and CO_2 laser methods. The ratio of the intensities of the symmetric and antisymmetric O–H stretches is different, however, from the two color scheme. Because the energy fluence of the IR-WEX is rather low, not all of the ions which absorb one photon are expected to dissociate and some frequency dependence in the signal could originate during the absorption of the second photon. This means that the relative intensities from the two color FCL and CO_2 laser spectrum are probably more reliable than that from the one color IR-WEX spectrum, since the CO_2 laser with its substantially higher energy fluence is expected to decompose all the vibrationally excited ions.

H_9O_4^+

The infrared spectrum of H_9O_4^+ is shown in Fig. 10. In H_9O_4^+ , the first solvation shell around the H_3O^+ core has been filled. This leads to a threefold symmetry so that a high level of degeneracy exists in the spectrum. Only two fundamentals are observed. The lower frequency one at 3644.9 cm^{-1} is assigned to the symmetric O–H stretch of the three outer H_2O groups. This is actually composed of a vibration of species A_1 and another of species E in point group C_{3v} , which are predicted to be separated by $\sim 1 \text{ cm}^{-1}$ with a relative intensity of 0.0–5.1 $\text{D}^2/(\text{Å}^2 \text{ amu})$, respectively.⁴⁰ The higher-frequency mode at 3730.4 cm^{-1} is assigned to the antisymmetric O–H stretch of the outer water groups and is also comprised of an A_1 and E species vibration. The

calculated splitting is again essentially zero with a relative intensity of 15.2–0.2 $\text{D}^2/(\text{Å}^2 \text{ amu})$, respectively.⁴⁰

The spectrum of $\text{H}_9\text{O}_4^+ \cdot \text{H}_2$ is shown in Fig. 5. Each of the two features seen in H_9O_4^+ has been split into a doublet. In each doublet, there is roughly a two-to-one intensity ratio with the smaller intensity peak on the red side. Comparison with the frequencies observed in H_9O_4^+ shows that the higher intensity member of each pair of the messenger spectra lies within 3 cm^{-1} of the IRMPD spectra. This led to the conclusion described in Refs. 48 and 49 that the H_2 messenger is localized near one of the three outer H_2O groups, causing the frequencies for that water group to be red shifted compared to the other two and have half the intensity of the unperturbed peaks.

An expansion of the 3730.4 cm^{-1} peak shows P , Q , and R branches emerging (Fig. 11). This is characteristic of a parallel band transition in a symmetric top. H_9O_4^+ is rigorously an oblate symmetric top with rotational constants from the calculated geometry of $A = B = 0.0876 \text{ cm}^{-1}$ and $C = 0.0453 \text{ cm}^{-1}$. The symmetry axis is perpendicular to the plane of the H_3O^+ core. For the A_1 species transition, this corresponds to having the antisymmetric stretch of the three H_2O groups in phase with each other. The transition of species E , which would give rise to a perpendicular band, is calculated to have almost no intensity.

Also shown in Fig. 10 are the SCF calculated scaled frequencies for the D_{3h} and C_{3v} forms of H_9O_4^+ , using a DZP basis set. The C_{3v} structure was calculated to be the lower energy geometry by 0.551 kcal/mol and frequencies corresponding to this structure are shown by dashed lines. The predicted transitions for the higher energy D_{3h} structure are denoted by solid lines. The primary differences between the two geometries (see Fig. 1) is that the C_{3v} geometry has a pyramidal H_3O^+ core and bent O–H–O bonds, whereas the D_{3h} geometry has a planar H_3O^+ core and linear O–H–O bonds. The calculated frequencies for the symmetric and antisymmetric O–H stretches of the H_2O moieties are practically the same for the D_{3h} and C_{3v} forms. Therefore, we cannot distinguish between these geometries based on the ab

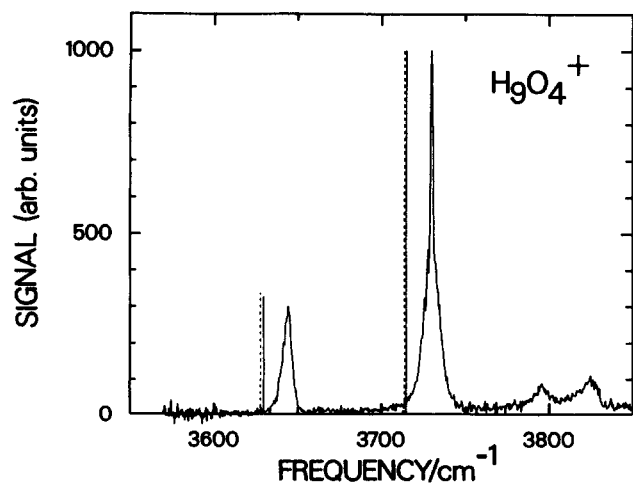


FIG. 10. The infrared spectrum of H_9O_4^+ obtained using the two color IRMPD approach. The dashed lines correspond to the lowest energy C_{3v} structure and the solid lines to the D_{3h} structure.

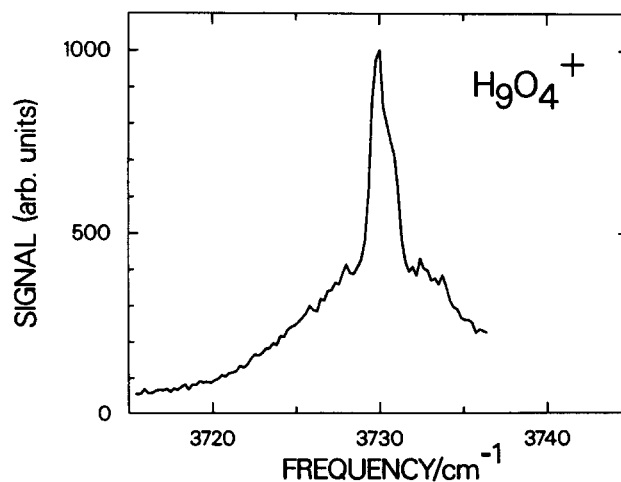


FIG. 11. Detail of the 3730 cm^{-1} feature in the IRMPD H_9O_4^+ spectrum.

initio frequencies. Table I compares the predicted frequencies for both structures with the observed frequencies taken both with and without a messenger.

Two features at higher frequency were also observed. Located at 3795.6 and 3824.1 cm^{-1} , these features also appear in the $\text{H}_9\text{O}_4^+ \cdot \text{H}_2$ messenger spectrum obtained previously. Since these bands lie at a significantly higher frequency than any fundamental band for the cluster as predicted by Remington and Schaefer,⁴⁰ the observed structure is probably due to overtones of lower-frequency modes, or more likely, combination bands of low-frequency vibrations with the intense O–H stretching modes.

Although an assignment of these features is not made at this time, temperature dependence studies of the spectrum of H_9O_4^+ suggest that these features do not come from either hot bands or structural isomers of the cluster. Contributions to the absorption spectrum by species other than H_9O_4^+ can be ruled out by recalling that both the parent ion beam and the products of the vibrational predissociation are mass selected. Any ion that would contribute to the absorption signal would have to have the same mass as H_9O_4^+ and fragment to the same mass as H_7O_3^+ after absorption. No evidence of contamination of the ion beam was observed in the mass spectra taken at various temperatures.

A Doppler limited spectrum for H_9O_4^+ from 3722 to 3738 cm^{-1} is now under investigation.

DISCUSSION

A few remarks on the results presented in the previous section are in order. First, note that the frequencies of the symmetric and antisymmetric O–H stretches of the outer H_2O groups increase with cluster size. This trend is shown in Fig. 12. The red shift of the frequency of the antisymmetric O–H stretch has decreased from 72 cm^{-1} in H_5O_2^+ to 26 cm^{-1} in H_9O_4^+ . The trend is also dramatic for the symmetric O–H stretch where the red shift decreased from 48 cm^{-1} in H_5O_2^+ to 12 cm^{-1} in H_9O_4^+ . It would be interesting to pursue this work to the larger cluster ions such as $\text{H}_{11}\text{O}_5^+$, where the additional water group is added to the next solvation shell, and compare the red shifts obtained then. We did the analogous experiment for the hydrogen cluster ions and found that the red shift in the H–H stretch decreased from 250 cm^{-1} in H_5^+ to 140 cm^{-1} in H_9^+ in which the first shell was filled.⁴³ As the cluster ion size was further increased from H_{11}^+ through H_{15}^+ , the red shift in the H–H stretch remained within 30 cm^{-1} of that seen for H_9^+ . Because the H_2 moiety depends on a perturbation from the H_3^+ core in order to become an allowed transition, it is likely that the H_2 units in the second solvation shell are not sufficiently perturbed to have a strong infrared intensity. Thus, the H–H stretch we observed for these larger hydrogen cluster ions almost certainly originates from the inner solvation shell. In the case of the water cluster ions, the situation should be different. The O–H stretches in free water are infrared allowed and thus do not depend on the proximity of a perturbative force to be observed. Thus, it may be that two sets of O–H stretches could be found. One would correspond to the

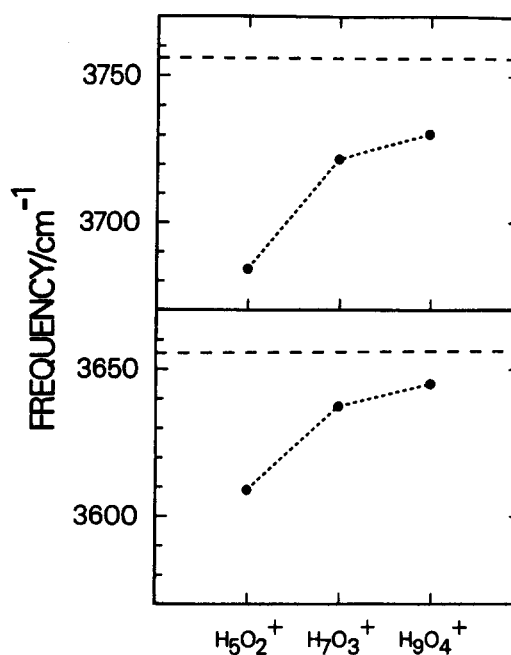


FIG. 12. The position of the antisymmetric (top) and symmetric (bottom) O–H stretches as a function of cluster size. The horizontal dashed lines are the locations of the respective O–H stretches in H_2O .

inner solvation shell and might have frequencies close to that found in H_9O_4^+ . The second would be shifted to the blue, closer to the frequencies found for free H_2O .

As to the validity of the messenger technique, we can say the method shows potential to be useful in obtaining a low-resolution scan of an otherwise unobservable ion. However, the choice of messenger is crucial in determining the degree of perturbation induced in the spectrum. For floppy molecules such as cluster ions, the shallowness of the potential makes these ions especially susceptible to significant structural and spectroscopic changes. In the case of H_5O_2^+ , the hydrogen messenger stabilized an H_3O^+ core changing the symmetry of the ion. This loss of symmetry led to two new bands corresponding to one free O–H bond of the H_3O^+ core and one O–H bond, also of the H_3O^+ core, to which the hydrogen messenger is loosely attached. For H_7O_3^+ , the frequency of the O–H bond, which was the site for the hydrogen messenger of the H_3O^+ core, shifted by 80 cm^{-1} compared to the IRMPD spectrum. This shift was reduced to only 9 cm^{-1} when neon was chosen as the messenger. In H_9O_4^+ also, significant changes were seen in the spectra with and without the hydrogen messenger. The presence of the H_2 near one of the H_2O groups broke the three fold symmetry and led to a splitting of each of the bands with a 2:1 intensity ratio. The red shift of the lower-frequency peak of each doublet was small (only 12 and 10 cm^{-1} for the symmetric and antisymmetric O–H stretches, respectively). Thus, it seems that the messenger technique would be more ideally suited to the study of rigid molecules that have deeper wells and higher barriers in the potential. Using a more inert messenger such as Ne or He would also minimize the perturbations introduced by the messenger. Since rigid molecules with higher dissociation energies are more difficult to study

using the IRMPD technique, these two techniques are complementary. The ideal candidate for the IRMPD method is a floppy molecule, such as a cluster ion, with many low-frequency modes, so that the quasicontinuum occurs at relatively low energies. A paucity of low-frequency modes might cause the beginning of the quasicontinuum to occur too high for the IRMPD technique to be feasible. This is the situation where using a messenger will give the least perturbation and give the best approximation to the low-resolution infrared spectrum.

On the other hand, the perturbation induced in the spectrum by the messenger can also be used to advantage. In systems without reliable structural information, the comparison of spectra taken with and without a messenger might be very revealing. Information on not only the structure of the cluster ion, but also on the available binding sites, could conceivably be obtained.

Ab initio theory predictions are also more reliable for rigid molecules with deep wells and high barriers in the potential. Cluster ions generally will be more floppy and have less well-defined structures. The structure calculated to be the lowest energy geometry may change as more sophisticated levels of theory are applied. This was seen in the case of H_5O_2^+ , where the early SCF, DZP basis calculation found the asymmetric C_s geometry to be the lowest in energy.⁴⁰ When the better CISD, DZP basis results were obtained, the symmetric C_2 geometry had become the lowest in energy by slightly less than 0.2 kcal/mol. This is probably near the accuracy limit of these kinds of calculations. The larger cluster ions are not accessible at the CISD level. Thus, Remington and Schaefer were limited to using SCF to calculate H_7O_3^+ and H_9O_4^+ . They calculate the C_s geometry of H_7O_3^+ to lie lowest in energy. Our experimental spectrum seems to indicate that the C_{2v} structure is actually the lower energy form. The energy difference calculated between the C_s and C_{2v} structures was only 0.516 kcal/mole. For H_9O_4^+ , the calculated frequencies for the C_{3v} and D_{3h} structures are nearly identical. Therefore, the observed spectrum does not aid in determining which geometry is actually the lower energy form. From these comparisons, it seems that *ab initio* theory has some difficulty in predicting relative energies for structures that are separated by only a few tenths of a kcal/mol as found in these cluster ions.

Besides the messenger technique and the two color IRMPD approach, a third approach was also tried to obtain the spectra. This was a one color multiphoton dissociation technique. Because H_5O_2^+ is bound most strongly, it would require three to four infrared photons of O–H stretching frequency to dissociate, whereas both H_7O_3^+ and H_9O_4^+ only need two photons. We were not able to obtain the H_5O_2^+ spectrum in this way, but the spectra of H_7O_3^+ and H_9O_4^+ were successfully obtained. H_5O_2^+ is particularly difficult, both because it has the strongest binding energy and because it is the smallest cluster ion and therefore has the fewest vibrational modes. Since the completion of this hydrated hydronium ion study, this technique has been successfully applied to study the ammoniated ammonium ions $\text{NH}_4^+ \cdot (\text{NH}_3)_n$ ($n = 3-10$).⁶⁸ Once again, this approach is limited to the larger size cluster ions. For $n = 1$ and 2, the

two color technique using a CO_2 laser was necessary in order to obtain the infrared spectra.

CONCLUSION

The study of the infrared spectroscopy of ionic clusters is an experimental challenge. The difficulty is caused largely by the very low ion densities obtained. In order to overcome this limitation, we have used "consequence" spectroscopy, where the consequence of absorbing an infrared photon is an observable event. The consequence which was utilized in these experiments was dissociation. The combination of a tandem mass spectrometer and a radiofrequency ion trap is ideal for the detection of dissociation products. Not only is there little to no background at the fragment ion mass, but also every fragment ion can be detected with nearly perfect detection efficiency. Three dissociation schemes have been described: messenger studies using hydrogen and neon, two color infrared multiphoton dissociation, and one color infrared dissociation. Results using these three techniques have been compared for the hydrated hydronium ions $\text{H}_3\text{O}^+ \cdot (\text{H}_2\text{O})_n$ ($n = 1, 2, 3$).

ACKNOWLEDGMENTS

We thank R. Remington and H. Schaefer for providing us with results of unpublished calculations. This work was supported by the Director, Office of Energy Research, Office of Basic Energy Sciences, Chemical Sciences Division of the U. S. Department of Energy under Contract No. DE-AC03-76SF00098. The F-center laser was on loan from the San Francisco Laser Center, a National Science Foundation Regional Instrumentation Facility, NSF Grant No. CHE79-16250 awarded to the University of California at Berkeley in collaboration with Stanford University.

¹For recent reviews, see C. I. Ratcliffe and D. E. Irish, in *Water Science Reviews* 2, edited by F. Franks (Cambridge University, Cambridge, 1986), p. 149; C. I. Ratcliffe and D. E. Irish, in *Water Science Reviews* 3, edited by F. Franks (Cambridge University, Cambridge, in press).

²R. S. Narcisi and A. D. Bailey, *J. Geophys. Res.* **70**, 3687 (1965).

³E. E. Ferguson, F. C. Fehsenfeld and D. L. Albritton, in *Gas Phase Ion Chemistry*, edited by M. T. Bowers (Academic, New York, 1979), Vol. 1, p. 45.

⁴I. Olovsson, *J. Chem. Phys.* **49**, 1063 (1968).

⁵J.-O. Lundgren and I. Olovsson, *J. Chem. Phys.* **49**, 1068 (1968).

⁶J.-O. Lundgren and I. Olovsson, in *The Hydrogen Bond: II. Structure and Spectroscopy*, edited by P. Schuster, G. Zundel, and C. Sandorfy (North-Holland, Amsterdam, 1976), Chap. 10.

⁷R. Attig and J. M. Williams, *Angew. Chem., Int. Ed. Engl.* **15**, 491 (1976).

⁸J. Roziere and J. M. Williams, *Inorg. Chem.* **15**, 1174 (1976).

⁹A. Nakahara, Y. Saito, and H. Kuroya, *Bull. Chem. Soc. Jpn.* **25**, 331 (1952).

¹⁰R. D. Gillard and G. Wilkinson, *J. Chem. Soc.* **1964**, 1640.

¹¹J. Rudolph and H. Zimmermann, *Z. Phys. Chem. (Frankfurt)* **43**, 311 (1964).

¹²J. Roziere and J. Potier, *J. Mol. Struct.* **13**, 91 (1972).

¹³A. S. Gilbert and N. Sheppard, *J. Chem. Soc., Faraday Trans. 2* **69**, 1628 (1973).

¹⁴J. M. Williams, in *The Hydrogen Bond: II. Structure and Spectroscopy*, edited by P. Schuster, G. Zundel, and C. Sandorfy (North-Holland, Amsterdam, 1976), Chap. 14.

¹⁵D. Schioberg and G. Zundel, *Can. J. Chem.* **54**, 2193 (1976).

- ¹⁶N. B. Librovich, V. P. Sakun, and N. D. Sokolov, *Chem. Phys.* **39**, 351 (1979).
- ¹⁷G. J. Kearley, A. N. Fitch, and B. E. F. Fender, *J. Mol. Struct.* **125**, 229 (1984).
- ¹⁸J. Q. Searcy and J. B. Fenn, *J. Chem. Phys.* **61**, 5282 (1974).
- ¹⁹G. M. Lancaster, F. Honda, Y. Fukuda, and J. W. Rabalais, *Int. J. Mass Spectrom. Ion Phys.* **29**, 199 (1979).
- ²⁰R. J. Beuhler and L. Friedman, *J. Chem. Phys.* **77**, 2549 (1982).
- ²¹P. Kebarle, S. K. Searles, A. Zolla, J. Scarborough, and M. Arshadi, *J. Am. Chem. Soc.* **89**, 6393 (1967).
- ²²A. J. Cunningham, J. D. Payzant, and P. Kebarle, *J. Am. Chem. Soc.* **94**, 7627 (1972).
- ²³Y. K. Lau, S. Ikuta, and P. Kebarle, *J. Am. Chem. Soc.* **104**, 1462 (1982).
- ²⁴M. Meot-Ner and F. H. Field, *J. Am. Chem. Soc.* **99**, 998 (1977).
- ²⁵H. A. Schwarz, *J. Chem. Phys.* **67**, 5525 (1977).
- ²⁶M. H. Begemann, C. S. Gudeman, J. Pfaff, and R. J. Saykally, *Phys. Rev. Lett.* **51**, 554 (1983).
- ²⁷M. H. Begemann and R. J. Saykally, *J. Chem. Phys.* **82**, 3570 (1985).
- ²⁸N. H. Haese and T. Oka, *J. Chem. Phys.* **80**, 572 (1984).
- ²⁹D.-J. Liu and T. Oka, *Phys. Rev. Lett.* **54**, 1787 (1985).
- ³⁰D.-J. Liu, N. H. Haese, and T. Oka, *J. Chem. Phys.* **82**, 5368 (1985).
- ³¹D.-J. Liu, T. Oka, and T. J. Sears, *J. Chem. Phys.* **84**, 1312 (1986).
- ³²V. Spirko and P. R. Bunker, *J. Mol. Spectrosc.* **95**, 226 (1982).
- ³³M. E. Colvin, G. P. Raine, H. F. Schaefer III, and M. Dupuis, *J. Chem. Phys.* **79**, 1551 (1983).
- ³⁴P. R. Bunker, W. P. Kraemer, and V. Spirko, *J. Mol. Spectrosc.* **101**, 180 (1983).
- ³⁵P. R. Bunker, T. Amano, and V. Spirko, *J. Mol. Spectrosc.* **107**, 208 (1984).
- ³⁶M. D. Newton and S. Ehrenson, *J. Am. Chem. Soc.* **93**, 4971 (1971).
- ³⁷M. D. Newton, *J. Chem. Phys.* **67**, 5535 (1977).
- ³⁸G. V. Yukhnevich, E. G. Kokhanova, A. T. Pavlyuchko, and V. V. Volkov, *J. Mol. Struct.* **122**, 1 (1985).
- ³⁹A. Potier, J. M. Leclercq, and M. Allavena, *J. Phys. Chem.* **88**, 1125 (1984).
- ⁴⁰R. Remington and H. F. Schaefer (unpublished results).
- ⁴¹R. J. Saykally and C. S. Gudeman, *Annu. Rev. Phys. Chem.* **35**, 387 (1984).
- ⁴²Recently this has been achieved for a few small stable ions. See J. Coe and R. J. Saykally, in *Ion and Cluster Ion Spectroscopy and Structure*, edited by John P. Maier (Elsevier, Amsterdam, 1989).
- ⁴³M. Okumura, L. I. Yeh, and Y. T. Lee, *J. Chem. Phys.* **83**, 3705 (1985) and M. Okumura, L. I. Yeh, and Y. T. Lee, *J. Chem. Phys.* **88**, 79 (1988).
- ⁴⁴W.-L. Liu and J. M. Lisy, *J. Chem. Phys.* **89**, 605 (1988).
- ⁴⁵D. F. Coker, R. E. Miller, and R. O. Watts, *J. Chem. Phys.* **82**, 3554 (1985).
- ⁴⁶M. F. Vernon, D. J. Krajnovich, H. S. Kwok, J. M. Lisy, Y. R. Shen, and Y. T. Lee, *J. Chem. Phys.* **77**, 47 (1982).
- ⁴⁷M. Okumura, L. I. Yeh, J. D. Myers, and Y. T. Lee, *J. Chem. Phys.* **85**, 2328 (1986).
- ⁴⁸M. Okumura, Ph. D. thesis, University of California, Berkeley, 1986.
- ⁴⁹M. Okumura, L. I. Yeh, J. D. Myers, and Y. T. Lee (to be published).
- ⁵⁰L. I. Yeh, Ph. D. thesis, University of California, Berkeley, 1988.
- ⁵¹V. J. Caldecourt, D. Zakett, and J. C. Tou, *Int. J. Mass Spectrom. Ion Phys.* **49**, 233 (1983).
- ⁵²S. G. Lias, J. F. Liebman, and R. D. Levin, *J. Phys. Chem. Ref. Data* **13**, 695 (1984).
- ⁵³H. A. Enge, *Rev. Sci. Instrum.* **30**, 248 (1959).
- ⁵⁴C. F. Giese, *Rev. Sci. Instrum.* **30**, 260 (1959).
- ⁵⁵C.-S. Lu and H. E. Carr, *Rev. Sci. Instrum.* **33**, 823 (1962).
- ⁵⁶S. Taya, I. Kanomata, H. Hirose, T. Noda, and H. Matsuda, *Int. J. Mass Spectrom. Ion Phys.* **26**, 237 (1978).
- ⁵⁷H. D. Zeman, *Rev. Sci. Instrum.* **48**, 1079 (1977).
- ⁵⁸Further details on the machine can be found in: S. W. Bustamente, Ph. D. thesis, University of California, Berkeley, 1983; S. W. Bustamente, M. Okumura, D. Gerlich, H. S. Kwok, L. R. Carlson, and Y. T. Lee, *J. Chem. Phys.* **86**, 508 (1987).
- ⁵⁹P. J. Robinson and K. A. Holbrook, *Unimolecular Reactions* (Wiley-Interscience, New York, 1972).
- ⁶⁰Available from the Quantum Chemistry Program Exchange, Department of Chemistry, University of Indiana, QCPE-234.
- ⁶¹H.-J. Werner, P. Rosmus, and E.-A. Reinsch, *J. Chem. Phys.* **79**, 905 (1983).
- ⁶²D. J. Swanton, G. B. Bacskay, and N. S. Hush, *Chem. Phys.* **107**, 9 (1986).
- ⁶³L. A. Pugh and K. N. Rao, in *Molecular Spectroscopy: Modern Research*, edited by N. Rao (Academic, New York, 1976), Vol. 2.
- ⁶⁴N. R. Daly, *Rev. Sci. Instrum.* **31**, 264 (1960).
- ⁶⁵G. Herzberg, *Molecular Spectra and Molecular Structure: II. Infrared and Raman Spectra of Polyatomic Molecules* (Van Nostrand-Reinhold, New York, 1945).
- ⁶⁶H. C. Allen, Jr. and P. C. Cross, *Molecular Vib-Rotors* (Wiley, New York, 1963).
- ⁶⁷W. Demtroder, *Laser Spectroscopy: Basic Concepts and Instrumentation* (Springer, New York, 1982), p. 87.
- ⁶⁸J. M. Price and M. W. Crofton (private communication).